THE JOURNAL OF PHYSICAL CHEMISTRY C

Article

pubs.acs.org/JPCC

Amplification in Light Energy Conversion at Q-CdTe Sensitized TiO_2 Photonic Crystal, Photoelectrochemical Stability in Se^{2-} Electrolyte, and Size-Dependent Type II Q-CdTe/CdSe Formation

Ali S. Nehme, Fatima Haydous, and Lara Halaoui*

Department of Chemistry, American University of Beirut, Beirut 110236, Lebanon

Supporting Information

ABSTRACT: This study investigates the ability of Se^{2-} redox electrolyte to separate the photoholes and stabilize Q-CdTe quantum dot solar cell with a liquid junction. We examined the photophysical and photoelectrochemical behaviors of Q-CdTe in two sizes, green-emitting dots of 2.3−2.7 nm diameter and red-emitting dots of 4 nm diameter, in the presence of alkaline Se^{2-} electrolyte prepared under inert atmosphere. Photoelectrochemical, absorbance, emission and emission quenching measurements revealed the presence of size dependence in Se^{2-} surface binding to Q-CdTe, growth of type II Q-CdTe/CdSe, and stability in the photoelectrochemical cell. Emission quenching measurements show that Se^{2-} scavenges the Q-CdTe photohole, with mechanisms that depended on size and quencher concentration. Binding of Se^{2-} to green-emitting Q-CdTe occurred with a greater binding constant compared to the red-emitting dots, resulting in formation of type II Q-CdTe/CdSe at the smaller core indicated in red-shifted absorbance and emission spectra with incremental Se^{2-} addition at room temperature. Photoelectrochemical measurements acquired at Q-CdTe sensitized nc-TiO_2 and TiO_2 inverse opal with a stop band at 600 nm, 600-i-TiO_2-o, in Se^{2-} electrolyte confirmed this redox species ability to scavenge the photohole and to protect Q-CdTe against fast photoanodic dissolution, with greater stability observed for the larger dots. Gains in the photon-to-current conversion efficiency attributed to light trapping were measured at Q-CdTe sensitized 600-i-TiO_2-o relative to nc-TiO_2.

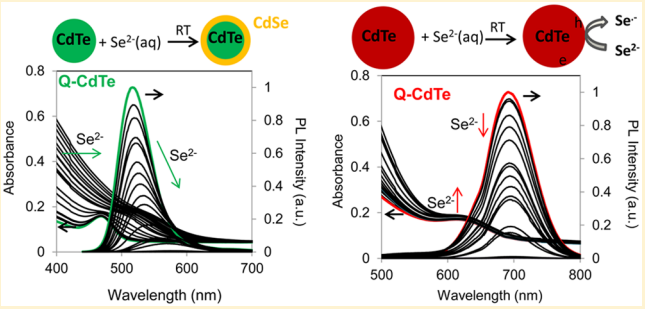

INTRODUCTION

Quantum dots (QD), semiconductor nanoparticles of size comparable to the exciton diameter, enjoy attractive properties that include tunable band gaps and band edges, high extinction coefficients, large dipole moments, relative ease of fabrication and assembly, and the potential of exceeding the thermodynamic limit for conversion of sunlight at a bulk semiconductor due to quantum confinement effects.[1−13] These properties have driven their use for quantum dot solar cells (QDSC) with the aim of increasing efficiency and reducing cost of power from photovoltaics.[1−13] In a widely investigated QDSC architecture, the QDs sensitize a nanostructured wide band gap semiconductor such as TiO_2 or ZnO in a liquid junction solar cell.[14,15] Several materials have been studied including CdS, CdSe, CdTe, ZnSe, InP, $CuInS_2$, PbS, alloys such as $CdSe_{1-x}Te_x$, and core/shell dots such as type II Q-CdTe/CdSe.[16] Efficiencies in the range of 6−7% have been reported using core/shell $CuInS_2$/ZnS on mesoporous TiO_2[17] or $CuInS_2$/CdS on TiO_2 nanotubes,[18] core/shell CdTe/CdSe on mesoporous TiO_2,[19] and $CdSe_xTe_{1-x}$ on TiO_2.[20] But they remain lower than the maximum efficiency of 13% reported at dye-sensitized solar cells (DSSC).[21]

Several obstacles need to be overcome for QDSC to achieve their promise. Different charge transfer and transport processes take place simultaneously and competitively in this QDSC architecture to yield charge separation and collection.[22,23] These include for instance photohole transfer to the redox species competing with hole reaction with the lattice, and electron transfer to the wide band gap semiconductor and its collection competing with back-electron transfer from the QD or the oxide semiconductor to the redox species. The redox electrolyte thus plays a key role in determining the efficiency, and in ensuring sufficient stability to allow fundamental studies and long-term operation of liquid junction QDSC.

CdTe is a direct II−VI semiconductor with a band gap of 1.45 eV that is optimal for solar energy conversion, and is highly stable in solid-state photovoltaic devices- making thin film CdTe solar cells second only to silicon single crystal solar cells on the global market. Q-CdTe would be of greater interest in studies of QDSC than the larger band gap cadmium chalcogenides CdS (2.4 eV) and CdSe (1.77 eV) because of its greater visible light absorbance, but its usefulness in QDSC with a liquid junction has been hindered by its significant instability in the photoelectrochemical medium.

The photohole in cadmium chalcogenides is very energetic and can oxidize the lattice itself.[24,25] This problem can be

Received: November 24, 2015
Revised: February 6, 2016
Published: February 25, 2016

DOI: 10.1021/acs.jpcc.5b11478
J. Phys. Chem. C 2016, 120, 4766−4778

overcome in the presence of a redox species capable of scavenging the hole faster than the photoanodic dissolution reaction. Sulfide electrolyte is commonly used to protect CdS and CdSe photoelectrodes from this oxidative process, but does not protect CdTe single crystals,[24] thin films,[26] or QDs.[25] CdTe-hole scavenging by S^{2-} though thermodynamically favorable does not kinetically compete with the reaction CdTe + 2h → Cd^{2+} + Te, and a CdS layer grows blocking photocurrent generation.[24−26] QDs are also not stable in the corrosive iodide/triiodide redox electrolyte commonly used in DSSC.[27] Kamat et al. reported that the following redox couples I^-/I_3^-, ferrocene/ferrocene$^+$, $K_4Fe(CN)_6/K_3Fe(CN)_6$, and Te^{2-}/Te_2^{2-} did not stabilize Q-CdTe.[25] Recently, we reported that Se^{2-} electrolyte prepared by reducing Se with $NaBH_4$ in NaOH under inert atmosphere stabilized thin CdTe films deposited by successive ionic layer adsorption and reaction (SILAR).[26] This led to appreciable photocurrent generation relative to sulfide, attributed to the ability of Se^{2-} to scavenge the CdTe-hole, with a possible slow growth of a protective thin overlayer containing Se that prevents further dissolution.[26]

In this study we investigate the ability of Se^{2-} to scavenge the hole and stabilize colloidal CdTe quantum dots, of size between 2.3 and 4 nm. The quantum dots have a more oxidizing hole with decreasing particle size due to quantum confinement effect and are thus more difficult to protect against fast anodic dissolution in the photoelectrochemical medium than large particles, thin films, or single crystals. We also examine the interaction between Se^{2-} and Q-CdTe dots leading to growth of type II quantum dots and its dependence on particle size. In addition, the study investigates the effect of the structure of the wide band gap oxide semiconductor designed as photonic crystal in enhancing light harvesting of Q-CdTe sensitized TiO_2 films in selenide electrolyte.

We investigated the quenching of emission of green-emitting and red-emitting colloidal 2.3 nm and ∼4 nm MPA-capped Q-CdTe dots by Se^{2-} and report: (1) binding of Se^{2-} on the surface of Q-CdTe is size-dependent, with a 7-times greater binding constant at 2.3 nm Q-CdTe compared to 4 nm Q-CdTe determined from the emission quenching data upon applying a model of equilibrium complex formation; (2) the difference in binding constant results in quick growth of type II Q-CdTe/CdSe dots at room temperature at the smaller core but not at the large core dots. This finding allows for a better fundamental understanding of the growth of type II QDs and its dependence on particles size, and of the dots surface transformation in the photoelectrochemical medium.

In addition to the photophysical study, we examined the photoelectrochemical behavior in selenide of Q-CdTe adsorbed on titania inverse opals and on nc-TiO_2 films and report: (3) that Se^{2-} can also stabilize CdTe QDs which have a more oxidizing hole than thin films reported earlier,[26] making the anodic dissolution more favored, yet hole scavenging by Se^{2-} can still compete preventing fast dissolution in the photoelectrochemical cell; (4) that gains in light harvesting occur when Q-CdTe is adsorbed on a TiO_2 photonic crystal compared to nc-TiO_2, near the absorption edges to both the blue and to the red of a stop-band centered at 600 nm. This presented a major improvement in light harvesting over similarly sensitized nc-TiO_2 films and compared to earlier work at SILAR-deposited CdTe thin film on nc-TiO_2 in the same electrolyte.[26] The gain in light harvesting is attributed to photonic effects trapping light in the inverse opal, and is our first study at Q-CdTe-on-inverse opal/liquid junction cell because the system could be stabilized with selenide to allow the measurement.

EXPERIMENTAL METHODS AND MATERIALS

Materials and Substrates. Fluorine-doped tin oxide coated glass (FTO, Solaronix, Switzerland, R = 15 Ω/sq, Solaronix) were used as electrodes. Sodium tellurite(IV), Na_2TeO_3 (99.5%, Alfa Aesar); $CdCl_2$ (99.99%, Aldrich);); Se powder (99.99%, Alfa Aesar); 3-mercaptopropionic acid, MPA (99+%, Acros); $NaBH_4$ (98%, Aldrich); suspensions of monodisperse 305 nm carboxylate-modified polystyrene spheres ($\sigma \leq 3\%$, 10% w/v in water, stored at 4 °C, Thermo scientific); polyoxy-ethylene(5)nonyl phenyl surfactant (Igepal CO-520, Aldrich); boric acid, H_3BO_3 (99.5%, Aldrich); ammonium hexafluorotitanate, $(NH_4)_2TiF_6$ (99.99%, Aldrich); titanium isopropoxide, $Ti(OCH(CH_3)_2)_4$ (98%, Aldrich); nanocrystalline titanium dioxide slurry, nc-TiO_2 (Ti−nanoxide T, 11% wt., $\langle d \rangle$ = 13 nm, Solaronix, Switzerland); 2-propanol (99%, Acros); HNO_3 (65%, Acros), NaOH (Aldrich), and deionized water (18 μΩ.cm, Nanopure Diamond) were used in this study.

Synthesis of MPA-Capped Q-CdTe. MPA-capped Q-CdTe was prepared from 0.019 g $CdCl_2$ and 0.0056 g Na_2TeO_3 dissolved in 100 mL, with the pH adjusted to 9 with 1 M NaOH, followed by adding 0.08 g of $NaBH_4$ and 14.2 μL of MPA and stirring for 10 min, and refluxing the clear solution at 100 °C. Aliquots were pipetted out at different reaction times to obtain Q-CdTe particles of varying size. Reaching the red-emitting solution requires about 9 h reflux. Characterization UV−vis and fluorescence spectra were acquired after diluting the QD solutions to have an absorbance peak around 0.3−04 through 1 cm path length.

Preparation of i-TiO_2-o and nc-TiO_2 Films and Sensitization. FTO electrodes were cleaned by ultrasonication in 2-propanol for 30 min and water for 20 min, followed by rinsing in water and drying in air. TiO_2 inverse opals were replicated using a previously reported liquid-phase deposition (LPD) procedure[28,29] from polystyrene photonic crystal template. The templates were assembled using evaporation induced self-assembly from a 0.05% suspension of 305 nm PS spheres containing 0.002% igepal, sonicated for 40 min, under ambient conditions at 55 °C (in Barnstead thermolyne oven, 48000). The PC templates were infiltrated by dipping for 5 min in 1.2% (w/v) titanium isopropoxide in ethanol containing 0.12% (w/v) nitric acid, and air-dried for 1 h, forming a seed layer. Films were then immersed vertically for 30 min at 50 °C in an aqueous solution of 0.2 M $(NH_4)_2TiF_6$ and 0.25 M H_3BO_3 at pH 2.9 adjusted with 1 M HCl. The films were rinsed with water and air-dried, then calcined at 400 °C for 8 h to yield i-TiO_2-o. Previous characterization revealed anatase TiO_2.[29] nc-TiO_2 films were deposited via the squeegee method from the TiO_2 particles slurry using scotch-tape to control the thickness. The solvent was dried at 80 °C for 1 min, and films were sintered at 400 °C for 1 h. Films thickness measured by profilometry (Ambiox X2 profilometer) was in the range of ca. 4.5−5.5 μm as indicated. To sensitize the films, 0.5 mL of the as-prepared QDs solution was solvent cast dropwise over a ∼2.5 cm^2 area of either nc-TiO_2 or i-TiO_2-o, and left to air-dry. Films were then annealed for 30 min at 300 °C under argon.

Preparation of Se^{2-} Electrolyte Solution. A 0.1 M Se^{2-} solution was prepared by adding 0.21 g of Se (s) and 0.20 g $NaBH_4$ to 27 mL deionized water purged with N_2(g). NaOH(s) was added to a pH of 12.8. A nitrogen blanket was

DOI: 10.1021/acs.jpcc.5b11478
J. Phys. Chem. C 2016, 120, 4766−4778

maintained above the solution for quenching or photoelectrochemical experiments to stabilize Se^{2-} against oxidation.

Fluorescence and Absorbance Measurements. Fluorescence measurements were acquired in quartz cuvette (Precision Cells Inc.) using a HORIBA Jobin Yvon FluoroLog W 3 spectro fluorometer (HORIBA Scientific) at 420 nm excitation using a 450 W xenon lamp as the excitation source. The excitation and emission slits were 5 nm wide. Fluorescence spectra were acquired at 90 deg relative to the excitation source and detected using a R-928P photomultiplier detector operating at 950 V. All measurements were carried out at room temperature (20 ± 2 °C), and data were acquired using 1 cm path length Fluorescence Quartz Cuvette with a screw cap for anaerobic work. Spectra were corrected for the instrument response. Q-CdTe solutions for quenching measurements by Se^{2-} were diluted by adding 1 mL of parent solution to 2.5 mL of water to have the same optical density of 0.16−0.17, unless otherwise indicated. Quenching experiments were performed under nitrogen by injecting 0.5 μL incremental additions with a syringe through a septum into the anaerobic cuvette under nitrogen. Control experiments showed a stable fluorescence over the time scale necessary to conduct the quenching experiments. The Se^{2-} quenching solution was prepared in nitrogen saturated deionized water. UV−visible absorbance spectra were recorded at room temperature in a 1 cm path length UV cuvette for anaerobic work, using a JASCO V-570 UV−vis/NIR Spectrophotometer (JASCO Europe s.r.l. Cremella (LC), Italy). For i-TiO_2-o films, the void structure was filled with water.

Photoelectrochemical Measurements. Photoelectrochemical measurements were acquired in a three-electrode quartz cell with a homemade Ag/AgCl electrode (KCl saturated) as a reference electrode, a 2 mm Pt wire as the counterelectrode, in a freshly prepared and deaerated alkaline 0.1 M Se^{2-}, with a nitrogen blanket maintained during measurements, using a Model 630A electrochemical workstation (CH Instruments). A 300 W xenon lamp (Model 66901 lamp housing, Oriel instruments) and a light dispersive 1/4 m grating monochromator (Oriel Instruments, Model 77200) with used for illumination. For photoaction spectra, amperometric plots were acquired at bias of −0.55 V vs (Ag/AgCl) at different wavelengths with 20 nm increments under chopped illumination and the photocurrent was determined after subtracting the dark current. The monochromatic incident-photon-to-current-conversion-efficiency (% IPCE) at a certain voltage is calculated according to

$$\%\ \mathrm{IPCE\ (at\ V)} = \frac{J_{@V}\left(\frac{\mathrm{A}}{\mathrm{cm}^2}\right)}{I_{@\lambda}\left(\frac{\mathrm{W}}{\mathrm{cm}^2}\right)} \times \frac{1240\ (\mathrm{eV{\cdot}nm})}{\lambda\ (\mathrm{nm})} \times 100$$

where J is the photocurrent density at the bias V vs Ag/AgCl, λ is the wavelength of light, and I is the light intensity at the electrode position. The light intensity was measured with a thermopile light detector and power meter (Model 70260, Oriel Instruments) with 10 s average measurements. The electrode position was determined at 100 mW/cm^2 illumination from the Xe lamp. A bias of −0.55 V was used as it yielded the greatest photocurrent and lowest dark current in cyclic voltammograms.

Determination of Q-CdTe Coverage. Q-CdTe coverage on i-TiO_2-o and nc-TiO_2 films sensitized with the same size dots was quantitatively evaluated by measuring the amount of Cd adsorbed on the surface using atomic absorption spectroscopy (SOLAAR coupled to ASX-510 autosampler). Q-CdTe was desorbed in 1 M HNO_3(aq) after photoelectrochemical measurements. A calibration curve was determined using Cd^{2+} solutions prepared in nitric acid. The amount of Cd adsorbed on a film was divided by the geometric area of the film. The normalized % IPCE was obtained by dividing % IPCE for each film by the amount of Cd in nmol/cm^2 adsorbed.

SEM imaging. SEM images of polystyrene PC and i-TiO_2-o films were obtained using a Tescan MIRA 3 FEG-SEM (CRSL, AUB).

RESULTS AND DISCUSSION

1. Photophysical Behavior of Q-CdTe in the Presence of Se^{2-} Hole Scavenger. *1.1. Optical Characterization of MPA-Capped Q-CdTe.* Absorbance and photoluminescence spectra of mercaptopropionic acid (MPA)-capped Q-CdTe aliquots taken at reaction times between 20 min and 7 h are presented in Figure 1. Absorbance spectra shown in Figure 1A feature blue-shifted absorption edges relative to bulk CdTe (855 nm, E_g = 1.45 eV) and peaks corresponding to the $1S_e-1S_{h3/2}$ excitonic transition, shifting to the red with increasing particle size, due to quantum size effects. The corresponding

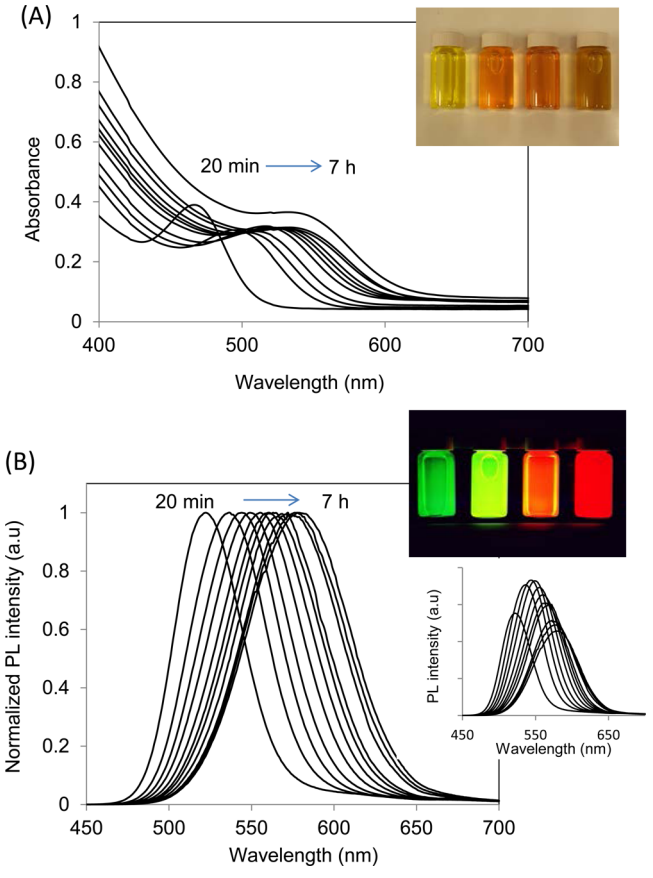

Figure 1. Absorbance (A) and photoluminescence (B) spectra of MPA-capped Q-CdTe aliquots taken at reaction times 20 min, 45 min, 1 h 30 min, 2 h, 2 h 30 min, 3 h, 3 h 30 min, 4 h, 5 h, 6 h, and 7 h, from left to right, of the same reaction. Photoluminescence spectra (inset) and normalized spectra are presented in Panel B. Photographs of Q-CdTe solutions of different sizes (inset of A) and when under 365 nm irradiation (inset of B); the brown-copper colored and red-emitting Q-CdTe solution was prepared separately at 9 h reflux time.

DOI: 10.1021/acs.jpcc.5b11478
J. Phys. Chem. C 2016, 120, 4766−4778

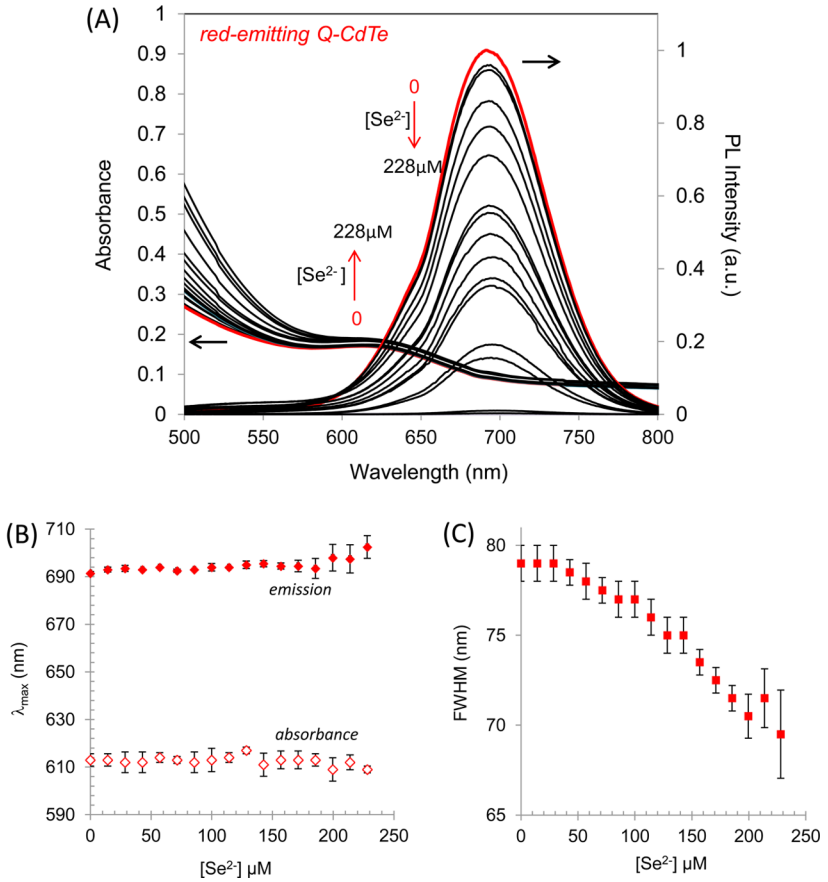

Figure 2. UV−visible absorbance (primary axis) and photoluminescence spectra (secondary axis) spectra of *red-emitting* Q-CdTe solution with λ_{abs} at 613 nm and λ_{em} at 692 nm, in the absence and presence of increasing amounts of Se^{2-}ions injected into the solution (0, 14, 28, 43, 57, 71, 86, 99, 114, 128, 142, 156, 171, 185, 199, 214, and 228 μM) (A). Plots of λ_{abs}, λ_{em} (B) and fwhm (C) as a function of Se^{2-} concentration.

emission spectra presented in Figure 1B, normalized to the peaks, show emission peaks near the absorbance edge indicating near band gap emission, similarly red-shifting with increasing particle size, and exhibiting a stokes-shift from the excitonic peak. The emission spectra before normalization in the (bottom right) inset of Figure 1B show that the emission intensity increased initially with increasing reaction time and peaked for green-emitting Q-CdTe with an excitonic peak at 504 nm and emission peak at 549 nm, then decreased with further growth. The solutions possessed a relatively broad spectral emission with a full-width-at-half-maximum (fwhm) in the range of 57−80 nm, attributed to the size distribution and surface effects from likely Te^{2-} anion vacancies—at the Cd:Te ratio used of 4:1—which can function as luminescent centers.[30,31] Photographs of Q-CdTe solutions of different sizes, including a brown-colored solution that emits in the red that took 9 h under reflux, are presented in the inset of Figure 1A. The photograph in the upper right inset of Figure 1B shows the emission colors of the same solutions under UV light.

The photophysical and photoelectrochemical behaviors were investigated for green-emitting and red-emitting Q-CdTe - termed green and red Q-CdTe. The size was calculated from the first excitonic peak position using the fitting equation given by Donegá et al. for sizes from 2 to 9.5 nm:[32]

$$E_g(d)(\mathrm{CdTe}) = 1.596 + 1/(0.137d^2 + 0.000d + 0.206)$$

where $E_g(d)$ is the energy of the first excited state in eV and d is the particle diameter in nm. Green Q-CdTe from different preparations exhibited an emission peak at 516−550 nm and excitonic peak between 468 and 504 nm yielding 2.33−2.65 nm diameter. Red Q-CdTe solutions emitted with λ_{em} at 679−690 nm and exhibited an excitonic peak at 612−615 nm corresponding to 3.93−3.98 nm diameter particles.

1.2. Photophysical Behavior of Q-CdTe Solutions in the Presence of Se^{2-}. The ability of Se^{2-} to scavenge Q-CdTe photoholes was investigated using fluorescence quenching measurements, and changes in absorbance and photoluminescence spectra were examined upon Se^{2-} additions to Q-CdTe solutions. Green and red Q-CdTe solutions were diluted to a peak absorbance of 0.16−0.17. The concentration was calculated from the extinction coefficient at 410 nm according to the method of Hens and co-workers:[33] ε_{410} ($cm^{-1}/\mu M$) = (0.0106 ± 0.0002) × d^3, where d is the diameter in nanometers. From A_{410} before adding Se^{2-} (which equaled 0.125 and 0.644 for green and red Q-CdTe, respectively), the concentrations of the diluted solutions were calculated to be 0.93 μM for green (2.33 nm) and 0.99 μM for red (3.95 nm) Q-CdTe.

Figure 2 shows the evolution of absorbance and photoluminescence spectra of red 3.95 nm Q-CdTe (λ_{abs} at 613 nm and λ_{em} at 692 nm) upon Se^{2-} injections up to 228 μM, along with plots of λ_{abs}, λ_{em}, and the emission peak fwhm as a function of Se^{2-} concentration. Addition of Se^{2-} increasingly quenched red Q-CdTe emission, but λ_{em} remained initially almost invariant, then red-shifting on average by only ∼6−11 nm with 200−228 μM Se^{2-} addition (Figure 2B). The fwhm equaled 79(±1) nm at low Se^{2-} concentrations then decreased

DOI: 10.1021/acs.jpcc.5b11478
J. Phys. Chem. C 2016, 120, 4766−4778

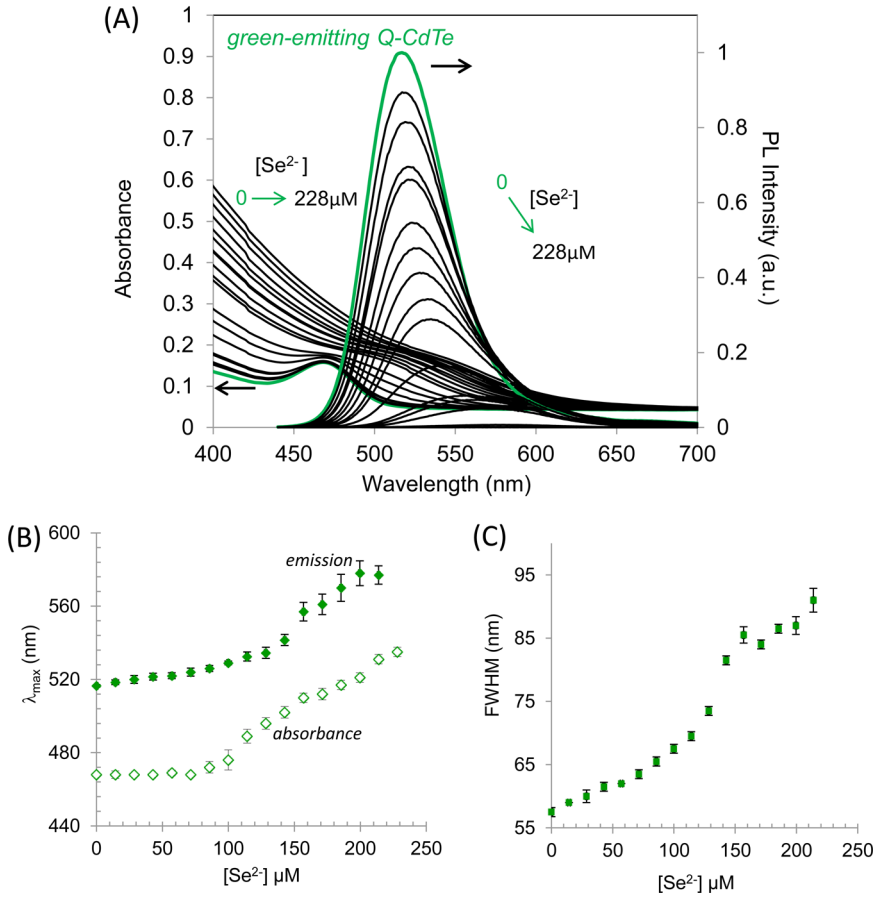

Figure 3. UV−visible absorbance (primary axis) and photoluminescence spectra (secondary axis) spectra of *green-emitting* Q-CdTe solution with λ_{abs} at 468 nm and λ_{em} at 517 nm, in the absence and presence of increasing amounts of Se^{2-}ions injected into the solution (0, 14, 28, 43, 57, 71, 86, 99, 114, 128, 142, 156, 171, 185, 199, 214, and 228 μM) (A). Plots of λ_{abs}, λ_{em} (B) and fwhm (C) as a function of Se^{2-} concentration.

down to 70(±2) nm (Figure 2C). λ_{abs} remained on average in the range 609−617 nm (Figure 2B) and the peak absorbance was almost constant with Se^{2-} additions. The increased absorbance at shorter wavelengths is attributed to Se^{2-} and was observed in absorbance spectra of Se^{2-} in water (Figure SI.1).

Smaller size green Q-CdTe exhibited a different photophysical behavior upon addition of Se^{2-}. Figure 3 shows the evolution of absorbance and emission spectra of 2.3 nm Q-CdTe ($\lambda_{abs.}$ at 468 nm and λ_{em} at 517 nm) with Se^{2-} injections up to 228 μM, and plots of λ_{abs}, λ_{em}, and the emission peak fwhm as a function of Se^{2-} concentration. Se^{2-} quenched green Q-CdTe emission. While at low concentrations up to 71 μM Se^{2-} the excitonic peak did not shift and the emission peak red-shifted by only ca. 6(±2) nm at 57 μM or 8(±2) nm at 71 μM, both peaks began to appreciably red-shift with more Se^{2-} injections following an S-shaped curve reaching a pseudoplateau (Figure 3B). The emission peak red-shifted by ~61(±5) nm with 214 μM Se^{2-}, λ_{em} of the significantly quenched peak at 228 μM Se^{2-} could not be accurately determined. The excitonic peak red-shifted by 63(±3) nm at 214 μM or 67(±3) nm at 228 μM Se^{2-} added. As it began to red-shift, the excitonic peak lost definition becoming increasingly featureless and the emission fwhm increased from 58(±1) nm to the range of 84(±1) nm to 91(±2) nm with 157−214 μM Se^{2-} additions following an S-shaped curve that mirrored the emission and absorption peaks' shifts (Figure 3C). Control experiments by injecting alkaline $NaBH_4$ without Se into Q-CdTe showed minimal decrease in emission and no change in excitonic peak position and absorbance (Figure SI.2). This decrease in emission could be caused by some hole scavenging by $NaBH_4$ but was not significant compared to the effect of Se^{2-}, a result in agreement with photoelectrochemical measurements (*vide infra*).

The quenching efficiency (ϕ_o/ϕ; ϕ is the quantum yield), taken as the ratio of peak emission intensities (I_o/I) for the same solution in the absence (I_o) and presence of the quencher (I), was plotted versus the concentration of Se^{2-}. The plots deviated from a standard linear Stern−Volmer plot ($I_o/I = 1 + K_{sv}[Se^{2-}]$) for both sizes with an upward curvature at high concentrations (Figure SI.3). The plots yielded a Stern−Volmer constant (K_{SV}) equal to 45.4 × 10^2 M^{-1} for red Q-CdTe from 0 to 57 μM (R^2 = 0.92) and 94.4 × 10^2 M^{-1} for green Q-CdTe from 0 to 57 μM (R^2 = 0.98), revealing a greater quenching efficiency for the smaller size Q-CdTe.

A deviation from Stern−Volmer linear behavior has been reported by El-Sayed and co-workers for Q-CdSe emission quenching by *n*-butylamine ($K_{sv,1}$ = 72.5 M^{-1}) with a downward curvature at higher quencher concentration, attributed to the presence of two surface binding sites one with less efficient quenching.[34] The Stern−Volmer plots for red and green Q-CdTe quenching by Se^{2-} can be seen to exhibit some downward curvature at intermediate quencher concentrations but then curved upward at higher concentration (Figure SI.3).

DOI: 10.1021/acs.jpcc.5b11478
J. Phys. Chem. C 2016, 120, 4766−4778

Kamat et al. analyzed the quenching of ZnO emission[30] by the hole scavengers I^-, SCN^-, and Se^{2-} and the quenching of Q-CdSe emission by p-phenylenediamine[35] by assuming equilibrium complex formation between particle and quencher. Following this analysis, assuming complex formation between Q-CdTe and Se^{2-}:

$$\text{Q} - \text{CdTe} + \text{Se}^{2-} \rightleftarrows \{\text{Q} - \text{CdTe}...\text{Se}^{2-}\} \quad K_{app} \tag{1}$$

This will yield the following equation:

$$\phi_o/(\phi_o - \phi) = \phi_o/(\phi_o - \phi') + \phi_o/\{(\phi_o - \phi')\ K_{app}[\text{Se}^{2-}]\} \tag{2}$$

where ϕ_o is the emission quantum yield in the absence of quencher, ϕ is the observed quantum yield at different concentrations of Se^{2-}, ϕ' is the quantum yield of the complex {Q-CdTe···Se^{2-}}, and K_{app} is the apparent binding equilibrium constant between Q-CdTe and Se^{2-}. In writing the equilibrium, we did not differentiate if Se^{2-} binds to MPA-free Cd sites or competes with surface-bound MPA. The plot of $I_o/(I_o - I)$ vs $1/[Se^{2-}]$ was linear over the full Se^{2-} concentration range for green Q-CdTe with K_{app} equal to 2.9×10^3 and $R^2 = 0.996$ (Figure 4), and the same when calculated up to 214 μM with R^2 = 0.996 (not including the significantly quenched peak at 228 μM; uncertainties in average peak intensity determination are reported in Supporting Information, Figure SI.3). On the other hand, the double reciprocal plot was not linear for red Q-CdTe at low Se^{2-} concentrations but can be fit to a linear line between 86 and 228 μM Se^{2-} with K_{app} equal to 4.0×10^2 M^{-1} and $R^2 = 0.97$ (Figure 4). For comparison, apparent binding constants equal to 715, 7100, and 1×10^4 M^{-1} were reported for ZnO binding with I^-, SCN^-, and H_2Se, respectively,[30] and 4.9×10^4 M^{-1} for 4 nm CdSe with *p*-phenylenediamine.[35]

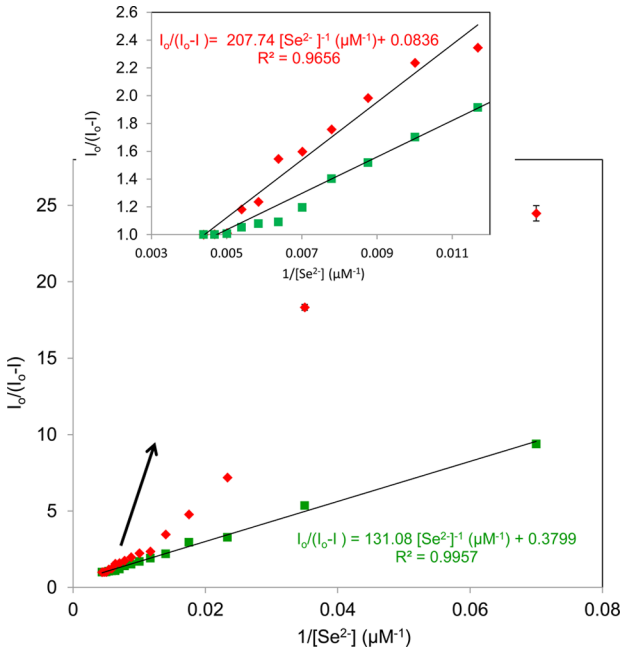

Figure 4. $I_o/(I_o - I)$ versus $1/[Se^{2-}]$ plots for green-emitting Q-CdTe, and for red-emitting Q-CdTe solutions.

Q-CdTe emission quenching by Se^{2-} is explained by assuming the presence of two mechanisms with onsets depending on particle size and Se^{2-} concentration. At low Se^{2-} concentrations, equilibrium 1 will be shifted toward Q-CdTe and Se^{2-}, with limited Se^{2-} bound to Q-CdTe sites. The quenching efficiency at 3.9 and 2.3 nm Q-CdTe followed a Stern–Volmer dependence at low Se^{2-} concentration, thus quenching could be collisional with unbound Se^{2-} scavenging the photogenerated hole from both red and green Q-CdTe, the redox potential of Se^{2-} being above the valence band edge (Scheme 1). The greater quenching efficiency at the small size

Scheme 1. Energy Level Diagram[a] of Bulk CdTe and TiO_2 on FTO at −0.55 V vs Ag/AgCl in Se^{2-}/Se_n^{2-} and the Redox Potential of the Anodic Dissolution Reaction[24]

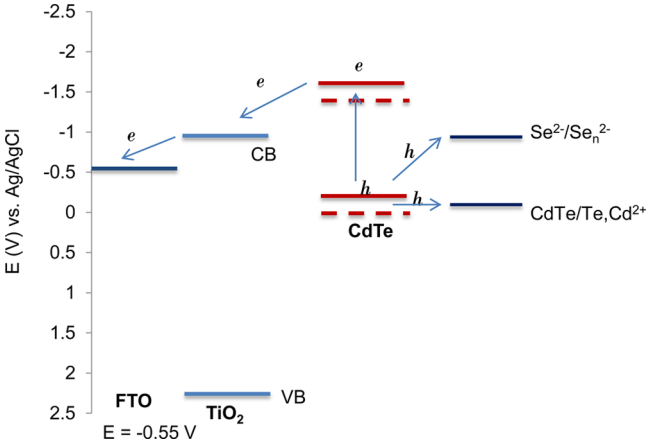

[a]Energy levels are taken from ref 24 as reported by Ellis et al. with the solid energy line for CdTe from photocurrent–voltage plots, and the dashed energy line for CdTe from Mott–Schottky plots.[24] The scheme is adapted from one presented earlier in ref 26.

Q-CdTe could be caused by a greater difference between the hole energy and the Se^{2-} redox potential, or built-in overpotential, due to quantum size effects, and to the carrier wave function extending more to the surface. At higher Se^{2-} concentrations the quenching efficiency for both Q-CdTe sizes increased nonlinearly with $[Se^{2-}]$ indicating predominance of a more efficient quenching, assumed to result from a bound Q-CdTe-Se state. Quenching of emission in this complex is supported by a linear relation between $I_o/(I_o - I)$ and $1/[Se^{2-}]$ over the full concentration range at 2.3 nm Q-CdTe, or with onset at higher quencher concentration at 3.9 nm Q-CdTe with its smaller binding constant (K_{app}) relative to the smaller core. At the 2.3 nm size Q-CdTe, eq 2 was also followed at low $[Se^{2-}]$, it is thus possible that some quenching occurred via a bound state, but Se-occupied sites would still be few and sporadic as the absorbance and emission peaks did not red-shift at these levels.

CdTe valence band and conduction band edges lie above those of CdSe with a bulk valence band offset of 0.57 eV,[36,37] shown in Scheme 2 (shaded inset). The red-shifts in absorbance and emission, the excitonic peak becoming featureless, the emission fwhm broadening, and the lower emission that accompanied high $[Se^{2-}]$ additions to 2.3 nm green Q-CdTe are characteristics of formation of type II Q-CdTe/CdSe core–shell particles, as presented in Scheme 2. Type II Q-CdTe/CdSe act as an indirect gap material with an effective energy gap smaller than either of the two materials; they were first reported in 2003 by Bawendi et al.[38] The red-shifted emission corresponds to recombination of a spatially separated exciton with the hole wave function mostly in CdTe,

DOI: 10.1021/acs.jpcc.5b11478
J. Phys. Chem. C 2016, 120, 4766–4778

Scheme 2. Sketch Representing Growth of Type II Q-CdTe/CdSe on Green-Emitting Q-CdTe Core but Not on Red-Emitting Q-CdTe in the Presence of Se^{2-} under Conditions Used in the Emission Quenching Experiment and Type II Band Edge Alignment of Bulk CdTe/CdSe

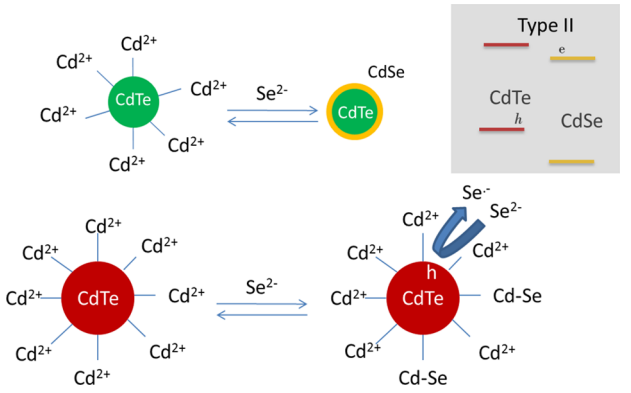

and the electron wave function increasingly localized in CdSe with increasing shell thickness.[38] Absorption of light of lower energy than Q-CdTe gap can occur forming a separated exciton, hence the red-shifted absorption. The oscillator strength decreases, and the excitonic transition becomes featureless consistent with the observations at the small core. On the other hand, a type II particle was not indicated at 3.9 nm Q-CdTe, since the emission quenching by Se^{2-} was not accompanied by red shifts in emission and absorbance. Scheme 2 shows quenching of the red Q-CdTe emission by Se^{2-} occurring in the unbound state. A 7-times smaller K_{app} between red Q-CdTe and Se^{2-} along with a 3-times greater surface area would result in equilibrium 1 not having shifted to appreciable Se-on-Q-CdTe coverage to lead to onset of type II QD characteristics at these concentrations. The small 6−11 nm red-shift in PL peak in the case of red Q-CdTe at the higher Se^{2-} concentrations is more likely due to size-selective quenching, with the smaller particles quenched more efficiently, which narrows the emission fwhm, since onset of type II particle formation would be indicated by a red shift in the excitonic peak and broadening in the emission fwhm. The absorbance of red Q-CdTe solution was followed up to 384 μM Se^{2-} after the emission was almost completely quenched, at the higher Se^{2-} concentrations the excitonic peak lost some definition and slightly red-shifted indicating increased Se coverage (Figure SI.4).

Reported preparations of type II Q-CdTe/CdSe showed to our knowledge that growth of the CdSe shell was achieved at temperatures of 90 °C in aqueous preparation[39] and higher than ∼200 °C[37,40,41] otherwise. Yu et al. followed the preparation via the pyrolysis of organometallic precursors in tri-*n*-octylphosphine oxide, and reported a red-shift in PL and absorbance upon heating to 190 °C at 52 min after first precursors' addition to Q-CdTe with an exciton peak at ∼650 nm.[37] The PL and absorbance red-shifts reached a plateau with a maximum red-shift of 52 nm attributed to a CdSe monolayer 0.4−0.5 nm thick,[37] and evolved in time in a trend similar to the evolution of the red-shift in emission and absorbance for 2.3 nm Q-CdTe at RT with incremental Se^{2-} additions. Chuang et al. reported CdSe shell growth at 225 °C on 3.4 nm Q-CdTe core with 140 nm red shift in the PL at 0.4 nm monolayer shell coverage.[40] The growth of a CdSe shell on the 2.3 nm core in this work occurred fast at room temperature and low concentrations, which could be explained by the size-dependent binding affinity between Q-CdTe and Se^{2-}. Because a Cd^{2+} source was not added, the adsorption reached full coverage with the dynamics reflected by a sigmoidal curve with a slower rate upon decreasing the fraction of unoccupied sites and the leveling off due to adsorption sites saturation. The ca. 61−67 nm red-shift observed, is consistent with other observation for CdSe monolayer growth.[37] Further growth would require addition of Cd^{2+}, or QD dissolution but the later would be accompanied by a blue-shift which was not observed at these illumination times.

In these reports of type II CdTe/CdSe particles,[37,39,40] the emission was observed to increase initially upon growth of a thin CdSe shell, contrary to our observations of emission quenching with proposed shell formation. Yu et al. reported that the quantum yield increased reaching a maximum for a monolayer then dropped with further growth.[37] Samanta et al. observed an increase in quantum yield of glutathione-capped Q-CdTe/CdSe before decreasing at more than 2 monolayers, the authors attributed the increase to reducing interfacial defects, and reported 3−5 times longer emission decay lifetimes at Q-CdTe/CdSe than at Q-CdTe.[39] Chuang et al. also observed an initial increase in quantum yield, followed by a slight decrease when a monolayer coverage was approached, and reported longer-lived PL with radiative lifetime increasing from 15 ns at the Q-CdTe core to 38 ns at a monolayer of CdSe on Q-CdTe.[40]

Anion vacancies create sites that are deep traps for conduction band electrons and act as luminescent centers.[30,31] Cd^{2+} addition has been shown to increase the photoluminescence of II−VI colloids[42,43] including CdTe colloid.[43] Synthesizing Q-CdSe at greater Cd to Se ratio reportedly increased the quantum yield believed to be due to Cd passivating surface traps that enhance nonradiative charge recombination.[35] Thus, the increase in emission quantum yield reported upon growth of a thin CdSe shell on Q-CdTe may have been caused by the Cd addition. The Q-CdTe colloid investigated here was prepared at a 4:1 Cd to Te ratio, thus the surface is expected to be Cd rich, and the CdSe shell formed upon Se^{2-} addition. Bawendi et al. reported significantly (120 times) longer radiative decay lifetime at Q-CdTe/CdSe than at Q-CdTe, resulting in low emission quantum yield because of slow recombination of the separated charges.[38] A longer-lived PL was also reported by Chuang et al. at Q-CdTe/CdSe particles[40] and others,[39,41] and results from a smaller overlap of the electron and hole wave functions after the carrier relax to the band edges of the type II particle.[41] A picture of complex formation between Cd-rich Q-CdTe and Se^{2-} with a lowered emission quantum yield is in agreement with the lower emission expected in type II Q-CdTe/CdSe core/shell because of separated wave functions.

Fast excitonic charge transfer (CT) has been reported to occur in type II particles in the subpicosecond time regime.[40,41] Chuang et al. observed using femtosecond pump−probe technique ultrafast electron transfer in type II Q-CdTe/CdSe, from a 3.4 nm Q-CdTe core to a thin CdSe shell.[40] The ultrafast electron transfer became measurable, occurring at subpicosecond time scale, as the quasi type II regime was approached at a monolayer shell thickness of 0.4 nm.[40] The formation of a CT state is in agreement with a longer-lived PL that was red-shifted from the core emission.[40] Ultrafast electron transfer from Q-CdTe to CdSe and longer-lived PL in the quasi type II Q-CdTe/CdSe particle is consistent with the quenching

DOI: 10.1021/acs.jpcc.5b11478
J. Phys. Chem. C 2016, 120, 4766−4778

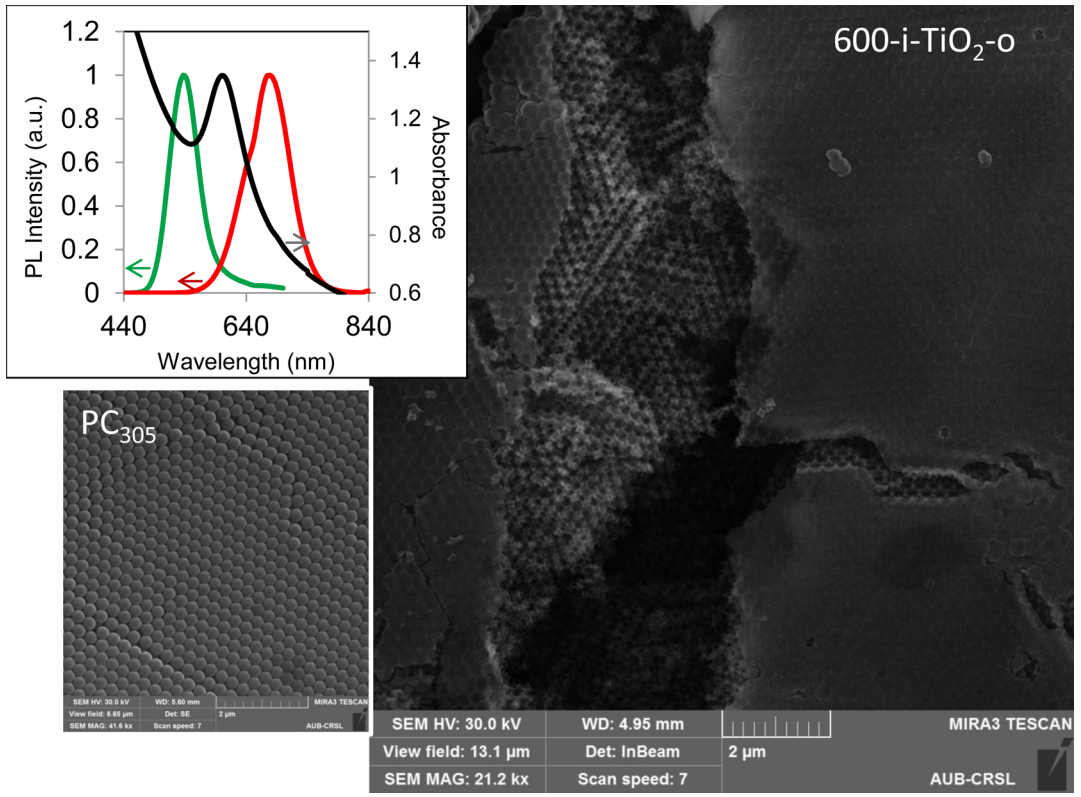

Figure 5. SEM images of TiO_2 inverse opal (600-i-TiO_2-o) and of polystyrene opal template assembled from 305 nm polystyrene spheres (PC_{305}), and photoluminescence spectra of green-emitting (green) and red-emitting (red) Q-CdTe solutions, and absorbance spectrum of i-TiO_2-o with the voids filled with water, showing the relative positions of the emission peaks to the blue and to the red to the stop-band peak at 600 nm.

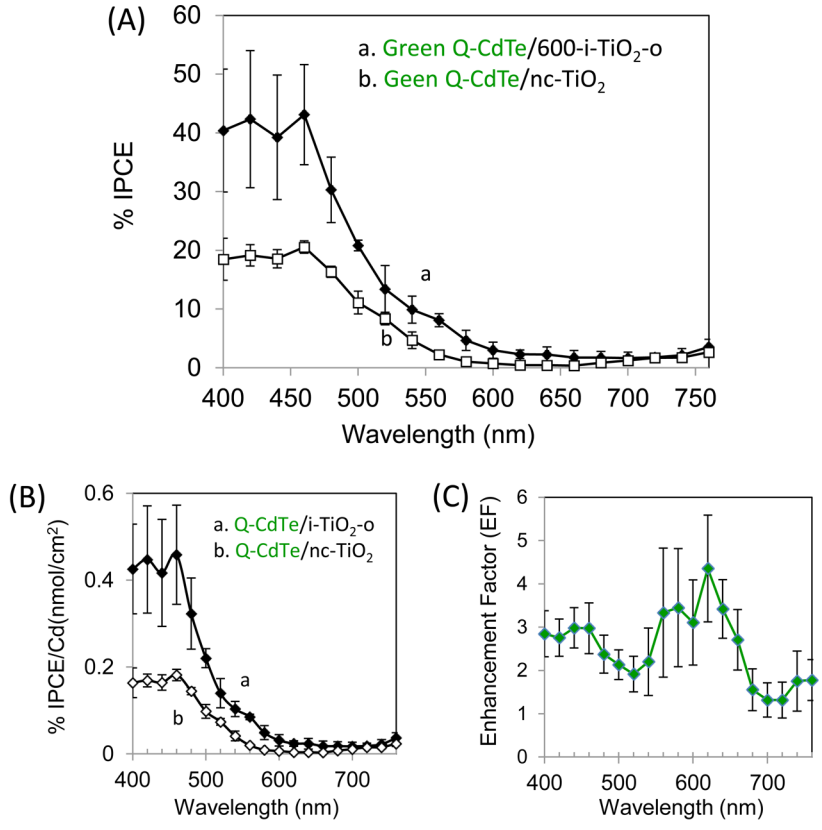

Figure 6. % IPCE vs wavelength plots at green-emitting Q-CdTe sensitized 600-i-TiO_2-0 and nc-TiO_2 (N = 3 each) (A). Normalized % IPCE spectra (B) and a plot of the enhancement factor vs wavelength (C).

DOI: 10.1021/acs.jpcc.5b11478
J. Phys. Chem. C 2016, 120, 4766−4778

of emission observed with addition of Se^{2-} to green-emitting Q-CdTe, and the model of complex formation leading to the growth of a CdSe shell reaching quasi type II regime at monolayer coverage. Prior to this bound state, collisional quenching can occur in an unbound state. We note that the quenching attributed to a bound state of complex formation between CdTe and Se^{2-} was observed before full monolayer was reached, as the quenching data could be fit to the model over the full Se^{2-} concentration range studied for the 2.3 nm core, but only at higher Se^{2-} concentration range for the 4 nm core. This can indicate that some charge separation occurs with partial CdSe coverage on CdTe. The results of this study show that the onset of type II regime at room temperature depends on core particle size, and on anion concentration, because of the dependence of the binding constant of Se^{2-} on the Q-CdTe size.

The CT state returning to the ground state via radiative and nonradiative routes was cited to occur at times from hundreds of nanoseconds to millisconds.[41] A fast charge separation in type II particles at the subpicosecond time scale, and low recombination rate of the separated charges makes these quantum dots attractive materials for photovoltaic devices,[41] where fast charge separation and slow recombination are essential toward increased efficiency of light energy conversion.

2. Photoelectrochemical Behavior of Q-CdTe-Sensitized nc-TiO_2 and i-TiO_2-o in Se^{2-} Electrolyte. *2.1. Inverse TiO_2 Opal and nc-TiO_2 Films Sensitized with Q-CdTe.* Figure 5 presents SEM images and absorbance spectra of an inverse TiO_2 opal with a stop band at 600 nm, termed 600-i-TiO_2-o, replicated from a polystyrene opal assembled from 305 nm spheres. The peak at 600 nm in water corresponds to a spherical void diameter of 201 nm according to the Bragg equation, in agreement with the 195 nm diameter measured by SEM, the shrinkage during assembly and infiltration is in agreement with earlier reports.[44,45]

Inverse TiO_2 opals and nc-TiO_2 films were sensitized with green-emitting Q-CdTe having an absorption edge at ~570 nm ($\lambda_{abs.}$ at 506 nm, $\lambda_{em.}$ at 546 nm, 2.65 nm size) and with red-emitting Q-CdTe with an absorption edge at ~710 nm ($\lambda_{abs.}$ at 615 nm, $\lambda_{em.}$ at 679 nm, 3.98 nm size), termed Q-CdTe-570 and Q-CdTe-710. The respective absorption edges thus lie to the blue or to the red of the inverse opal stop band. Photoluminescence spectra of green and red Q-CdTe sensitized i-TiO_2-o and nc-TiO_2 films are presented in Figure SI.5. Sensitization was achieved by solvent casting followed by annealing to 300 °C under argon.[46] The annealing step improved the photocurrent, possibly removing the linker and enhancing interfacial charge transfer. The carboxylate group of the bifunctional MPA ligand must have facilitated initial Q-CdTe attachment to TiO_2.

2.2. Photoelectrochemical Behavior and Stability of Q-CdTe-Sensitized i-TiO_2-o and nc-TiO_2 in Se^{2-} Electrolyte. Figure 6 presents average incident-photon-to-current conversion efficiency (%IPCE) vs wavelength plots at three films each of Q-CdTe-570-sensitized 600-i-TiO_2-o (4.4 ± 0.5 μm) and nc-TiO_2 (5.3 ± 0.6 μm) in 0.1 M Se^{2-} electrolyte. Relatively appreciable photocurrents were measured in the presence of Se^{2-}. Average %IPCE at Q-CdTe/600-i-TiO_2-o equaled 10% at 540 nm, 13.4% at 520 nm, and 40.3% at 460 nm; or equaled 4.7%, 8.4%, and 20.5%, respectively, at Q-CdTe/nc-TiO_2. This is an improvement in light harvesting for Q-CdTe on i-TiO_2-o, by 1.6-fold on average at 540 nm and 2.6-fold at 460 nm, compared to earlier work at a 10-layer CdTe film deposited by SILAR on nc-TiO_2 with an absorption edge at ~800 nm.[26] This 10-layer CdTe/nc-TiO_2 film yielded % IPCE of 6.12% at 540 nm and 15.6% at 460 nm in 0.1 M Se^{2-}, while minimal photocurrents and instability were observed in sulfide.[26] For comparison, a ~ 0.5%IPCE has been reported at 3.2 nm Q-CdTe sensitized nc-TiO_2 in 0.1 M Na_2S at 500 nm (see Figure 5 of ref25).[25]

The photocurrent onset at Q-CdTe-570/nc-TiO_2 in Se^{2-} was measured at ~580 nm near the QD absorbance edge. This indicates absence of significant dissolution or core/shell formation during this measurement, as these processes would have resulted in a blue-shift or a red-shift in the photocurrent onset, respectively. Q-CdTe-570/nc-TiO_2 in alkaline $NaBH_4$ in the absence of Se yielded significantly smaller photocurrent and a blue-shifted photocurrent onset at 480−500 nm indicating Q-CdTe dissolution. The photocurrent in $NaBH_4$ may indicate a degree of hole scavenging but unremarkably compared to Se^{2-}, in agreement with emission quenching.

The photoaction spectra of Q-CdTe-570/600-i-TiO_2-o showed greater %IPCE relative to similarly sensitized nc-TiO_2 down to ~660 nm, attributed to light trapping in the inverse opal rather than to a significant red-shift due to core/shell growth (*vide infra*). %IPCE normalized to the amount of Cd, which equaled 95 ± 7 nmol/cm^2 and 113 ± 3 nmol/cm^2 at i-TiO_2-o and nc-TiO_2 films, respectively, show greater light energy conversion per Q-CdTe at the inverse opal, with an average EF of 3.3 ± 1.5 at 560 nm or 3.4 ± 1.4 at 580 nm (Figure 6). The gain remained significant 200 nm to the blue of the stop-band center (Figure 6). A significant gain was also measured to the red of the stop band, but the photocurrents were minimal since green Q-CdTe did not appreciably absorb at these energies, and at the center of the stop band- albeit smaller than to either side of the gap.

Q-CdTe-710-sensitized nc-TiO_2 and 600-i-TiO_2-o yielded greater photocurrent conversion efficiency than Q-CdTe-570 sensitized films in the red wavelength range, as expected from their greater absorbance. Photoaction spectra of two films each of 600-i-TiO_2-o and nc-TiO_2 sensitized with Q-CdTe-710, with 93 ± 3 nmol/cm^2 and 169 ± 12 nmol/cm^2 Cd, respectively, are presented in Figure SI.6. % IPCE normalized to the amount of Cd showed higher conversion efficiency per adsorbed red Q-CdTe at the inverse opal to the blue and to the red of the stop-band relative to nc-TiO_2. Notably, the photoaction spectra at both sensitized titania structures exhibited lower % IPCE in the ca. 600 nm range followed with an increase at longer wavelengths. The cause of this drop at nc-TiO_2 films is not evident since the films are nonscattering, but the dip was significantly greater at 600-i-TiO_2-o as clearly seen in the normalized % IPCE spectra (Figure SI.6) and is attributed to reflection of light within the stop band frequencies.

Gains were thus observed to both the blue and to the red of the 600-i-TiO_2-o stop-band sensitized with Q-CdTe. Average gains were in the range 2.2−3.1 fold for Q-CdTe-710 at 700−740 nm near its absorbance edge to the red of the stop-band center, or 3.3−3.4 fold at Q-CdTe-570 at 560−580 nm near its absorbance edge to the blue of the stop band center. Significant amplification in light energy conversion were reported at Q-CdS/i-TiO_2-o[44] and at Q-CdSe deposited by SILAR on i-TiO_2-o[45] to the blue of the stop band center, while lower gains were previously observed to the red.[44] A maximum average EF of 4.7 for Q-CdS/i-TiO_2-o was reported at the blue edge of the stop band or 1.4−1.8 at the red edge when the absorbance edges coincided with the absorbance edges,[44] and an average EF of

DOI: 10.1021/acs.jpcc.5b11478
J. Phys. Chem. C 2016, 120, 4766−4778

6.7-fold was reported at Q-CdSe films on i-TiO_2-o to the blue of the stop band.[45] The gain has also been consistently observed to extend over a wide frequency range to the blue of the stop band center.[44,45] The amplification in light energy conversion is attributed to photonic effects localizing light in the inverse opal at these frequencies, and its extension significantly to the blue could be caused by disorder increasing internal light scattering. The smaller gain observed to the red than to the blue of the stop band in earlier report at Q-CdS/i-TiO_2-o was attributed to disorder lowering the gain in the dielectric band more than within the air-band,[44] but experiments involved photonic crystals prepared with different stop bands, and thus the effect of disorder on the red and blue edges' amplification of the same photonic crystal still requires systematic study. The gain did not drop below one within the stop band frequencies at Q-CdTe-570/600-i-TiO_2-o, possibly indicating a degree of light localization for light that can propagate because of disorder—which introduces energy states within the stop band, and this observation is also consistent with earlier ones at Q-CdS/i-TiO_2-o.[44]

The photoelectrochemical stability of red- and green-emitting Q-CdTe in 0.1 M Se^{2-} was examined by monitoring photocurrent generation with time at −0.55 V bias and 500 nm illumination. Figure 7 shows chronoamperometry curves at Q-CdTe-570/600-i-TiO_2-o (A) and Q-CdTe-710/600-i-TiO_2-o (B) illuminated for ∼2 h, and the respective insets show $i-t$ curves acquired at these films under chopped illumination,

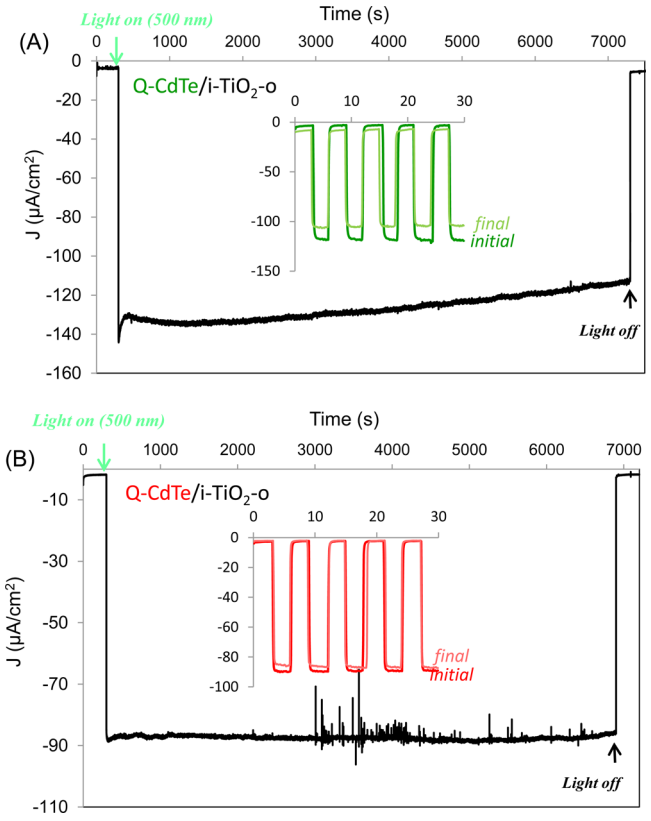

Figure 7. Chronoamperometry plots at green-emitting Q-CdTe sensitized i-TiO_2-o (A) and red-emitting Q-CdTe sensitized i-TiO_2-o (B) under continued illumination (λ = 500 nm) in alkaline 0.1 M Se^{2-} electrolyte. The insets show chronoamperometry plots acquired under chopped illumination in the same photoelectrochemical cell before and after the ∼2 h long current measurements.

before and following the plots under continuous illumination, in the same Se^{2-} solution. The $i-t$ plot under continued illumination in Figure 7A at Q-CdTe-570/i-TiO_2-o shows a photocurrent spike upon turning the light on, after 300 s in the dark under bias. The photocurrent after 1 h 50 min illumination decreased by 17% relative to the photocurrent after 100 s illumination, or by 24% relative to the photocurrent at light onset. A 14% drop was measured between initial and final $i-t$ curves presented in the inset of Figure 7A. On the other hand, the $i-t$ curve at Q-CdTe-710/i-TiO_2-o in Figure 7B showed the photocurrent to decrease by only 2.7% after 1 h 50 min continued illumination. The current was measured to drop by 4.2% from $i-t$ curves acquired under chopped illumination before and after the ∼2 h stability run, presented in the inset of Figure 7B.

Photoelectrochemical stability tests were also conducted at sensitized nc-TiO_2 films in Se^{2-} (Figure SI.7). The $i-t$ curve at Q-CdTe-570/nc-TiO_2 shows a photocurrent drop by 21% after ∼1 h 50 min continuous illumination relative to the photocurrent at light onset, or by 12−19% when measured from $i-t$ curves acquired before and after the 2 h $i-t$ run. The dark current also changed with time. At Q-CdTe-710/nc-TiO_2, the $i-t$ curve under continued illumination showed an initial increase in photocurrent upon turning the light on, followed by 2.5% decrease after 1 h 50 min illumination relative to the photocurrent at 100 s after illumination. A 7.7−10.9% decrease was measured in $i-t$ curves before and at the end of the 2 h $i-t$ run.

A greater electrochemical stability is thus indicated for the larger size ∼4 nm Q-CdTe in Se^{2-} in the dark and under illumination, despite greater hole scavenging efficiency by Se^{2-} from the smaller QD. In an earlier study, CdTe thin films with an absorbance edge at 800 nm on nc-TiO_2 exhibited a photocurrent decrease by only 5−8% after 2−3 h illumination at 500 nm in Se^{2-} indicating appreciable photostability, even as Se was shown to be incorporated in the films.[26] The earlier result is consistent with the greater photocurrent stability of the larger size QD, and showed that incorporation of Se did not block photocurrent generation.

The ability of Se^{2-} redox species to protect Q-CdTe in the photoelectrochemical medium will depend on a competition between the rates of the hole scavenging reaction 3:

$$CdTe(h^+) + Se^{2-} \rightarrow Se^{-\bullet} + CdTe \quad (3a)$$

$$CdTe(h^+) + Se^{-\bullet} + Se^{2-} \rightarrow Se_2^{2-} + CdTe \quad (3b)$$

and the anodic dissolution reaction 4:

$$CdTe(2h^+) \rightarrow Cd^{2+} + Te^0 \quad (4)$$

The reduction potential of the reaction Te + 2e + Cd^{2+} → CdTe has been reported at −0.14 V vs SCE, and the valence band edge of bulk CdTe in selenide was measured either at −0.25 V using current−voltage plots or at −0.05 V from Mott−Shottky plots by Ellis et al.,[24] making the photoanodic dissolution reaction either thermodynamically unfavorable at bulk CdTe or occurring with a built-in overpotential of 90 mV. This is considerably smaller than the driving force for hole scavenging by Se^{2-} (the Se^{2-}/Se_n^{2-} reduction potential is at −0.95 V vs SCE) as shown in Scheme 1.[24,26] The driving force, or built-in overpotential, is size-dependent, increasing for both reactions with decreasing particle size, though quantum size effect on the valence band edge energy is not very large because of the greater hole effective mass ($0.35m_o$) compared to the

DOI: 10.1021/acs.jpcc.5b11478
J. Phys. Chem. C 2016, 120, 4766−4778

electron ($0.11m_o$).[46] It is possible that because of the significantly larger built-in overpotential for reaction 3 than reaction 4, the effect of size is greater on the dissolution reaction. Overlayer growth in eq 5 will also affect the electrochemical behavior of Q-CdTe:

$$\text{Q–CdTe–Cd} + \text{Se}^{2-} \rightarrow \text{Q–CdTe/CdSe} \quad (5)$$

this reaction was shown in this study to be more favorable at the small size dots.

Q-CdTe in the photoelectrochemical cell is under different surface, solution, and illumination conditions than in emission quenching measurements. The QDs were subjected to annealing to remove the linker when attached to TiO_2 and are under illumination for longer time under bias in contact with higher—0.1 M—Se^{2-} concentration. The photoelectrochemical results however can be explained in accordance with the photophysical behavior taking into account these differences. The initial increase in photocurrent upon turning the light on after the green Q-CdTe films were in Se^{2-} in the dark can be due to thin shell growth increasing absorbance and charge separation. Ultrafast electron transfer observed in Q-CdTe/CdSe with a thin shell[40] is consistent with the attribution that initial shell growth can increase the photocurrent by increasing charge separation. The photocurrent drop that followed under illumination could have resulted from some Q-CdTe dissolution with time in the light, accompanying growth of a CdSe (or $CdTe_{1-x}Se_x$) overlayer that stabilizes the QD core from further dissolution. Growth of a thick shell though may also be accompanied by a decrease in photocurrent if it reduces the rate of hole scavenging across a thicker shell, the hole being localized in the core. The greater photocurrent stability of red Q-CdTe could be attributed to a slower anodic dissolution and a slower overlayer growth in 0.1 M Se^{2-}.

Photoluminescence spectra after the photoelectrochemical stability test (Figure SI.8) showed similar behavior at red and green Q-CdTe. As-sensitized Q-CdTe-570—with λ_{em} at 537 nm—on 600-i-TiO_2-o emitted at 522 nm, and the emission peak red-shifted by 13 nm after the ~2 h illumination in 0.1 M Se^{2-} with the intensity quenched by ~5-fold. The emission quenching indicated Se^{2-} binding to the surface, but the red shift was smaller than the 61 nm red shift measured with thin CdSe shell. The small red shift, in 0.1 M Se^{2-}, is consistent with assuming that some CdTe dissolution occurs during continued illumination. Green Q-CdTe/nc-TiO_2 emitted at 547 nm, and its emission was quenched by 11-fold after ~2 h under illumination and the peak blue-shifted slightly to 542 nm, consistent with some dissolution taking place with time. As-sensitized red Q-CdTe—with λ_{em} at 679 nm—on i-TiO_2-o emitted at 673 nm and was quenched by 64-fold after ~2 h in the light with a 10 nm red-shift. Red Q-CdTe/nc-TiO_2 emitted at 676 nm, its emission was quenched by ~19-fold, and blue-shifted to 666 nm. Despite a significantly more stable photocurrent at the red Q-CdTe/i-TiO_2-o than the green-sensitized film, the observed quenching of emission, and the red-shifts were similar at both inverse opal sensitized films. An explanation could be that the red-shifted emission at red Q-CdTe is a result of size-dependent quenching and adsorption of Se, but with less dissolution, therefore a smaller photocurrent drop. The characterization of Q-CdTe surface changes during photoelectrochemistry in the presence of Se^{2-} as a function of QD size and wide band gap semiconductor structure will require further investigation.

CONCLUSIONS

We examined in this study the photophysical and photoelectrochemical behavior of green-emitting and red-emitting Q-CdTe quantum dots in the size range 2.3–4 nm in the presence of Se^{2-} and the effect of a photonic crystal structure on the light harvesting efficiency of Q-CdTe in selenide. The main findings are summarized as follows: (1) The binding of Se^{2-} on the Q-CdTe surface is determined to be size dependent, with a 7-times greater binding constant for 2.3 nm Q-CdTe compared to 4 nm Q-CdTe, as determined from emission quenching data. (2) The greater binding constant of Se^{2-} to the small core leads to fast growth of a CdSe shell, at room temperature and low Se^{2-} concentrations, leading to type II CdTe/CdSe characteristics, a process that is slower to occur at the large size dots. (3) Se^{2-} can scavenge the Q-CdTe dots photohole and this reaction can compete with anodic dissolution in the photoelectrochemical medium thus stabilizing the CdTe quantum dots during illumination but with a greater stability for the red-emitting dots. (4) Adsorbing Q-CdTe on the surface of a TiO_2 inverse opal leads to gains in the photon-to-light conversion efficiency compared to nc-TiO_2 films, at frequencies to the red and to the blue of the stop band gap, and this effect is likely caused by light trapping inside the photonic crystals. The size dependence in Se^{2-} binding on the QD surface, leading to a size dependent dynamics of growth of type II dots at room temperature, is an important fundamental finding to understand the factors that govern growth of type II dots in solution and their surface transformation in the photoelectrochemical cell. The gains in light harvesting that resulted from adsorbing the QDs on i-TiO_2-o presents a major improvement in the light harvesting efficiency compared to Q-CdTe adsorbed on nc-TiO_2 or to our earlier report of CdTe thin films on nc-TiO_2.[26] Further studies need to explore the surface changes that occur in the photoelectrochemical cell as a function of quantum dot size, surface modification, and support structure and the charge separation and transfer dynamics accompanying these transformations. Understanding the chemical interactions between quantum dots and redox species and the physical changes to the dots under bias and illumination are essential for a comprehensive understanding of the photoelectrochemical behavior of quantum dot solar cells with a liquid junction and for overcoming limitations facing increasing efficiency and long-term stability.

ASSOCIATED CONTENT

Supporting Information

The Supporting Information is available free of charge on the ACS Publications website at DOI: 10.1021/acs.jpcc.5b11478.

UV–visible absorbance spectra of Se^{2-} alkaline solutions in water with increasing volume additions of the electrolyte solution Se^{2-}, absorbance and emission spectra of green-emitting Q-CdTe solutions with increasing additions of $NaBH_4$/NaOH solution, Stern–Volmer plots I_0/I versus Se^{2-} for green-emitting and red-emitting Q-CdTe solutions along with the uncertainties in peak intensities, absorbance spectra of red-emitting Q-CdTe with Se^{2-} additions up to 348 μM, PL spectra of nc-TiO_2 and 600-i-TiO_2-o films sensitized with green- or red-emitting Q-CdTe, %IPCE and normalized %IPCE and enhancement factor plots versus wavelength for red-emitting Q-CdTe sensitized 600-i-TiO_2-o compared to sensitized nc-TiO_2, stability tests of chronoamperometry

DOI: 10.1021/acs.jpcc.5b11478
J. Phys. Chem. C 2016, 120, 4766–4778

plots for green- and red-emitting Q-CdTe sensitized nc-TiO_2 films with ∼2 h illumination, and PL spectra of green and red Q-CdTe on nc-TiO_2 or on i-TiO_2-o before and after the stability tests in the photoelectrochemical cell (PDF)

AUTHOR INFORMATION

Corresponding Author

*(L.H.) E-mail: Lara.Halaoui@aub.edu.lb.

Notes

The authors declare no competing financial interest.

ACKNOWLEDGMENTS

We thank the Munib and Angela Masri Institute for Energy and Natural Resources at AUB (Grant 2013-15) and the University Research Board at the American University of Beirut (Grant 2011-13) for financial support of this research. We acknowledge the K. Shair Central Research Science Laboratory (CRSL) in the Faculty of Arts and Sciences at AUB for access to instruments.

REFERENCES

(1) Mora-Seró, I.; Giménez, S.; Fabregat-Santiago, F.; Gómez, R.; Shen, Q.; Toyoda, T.; Bisquert, J. Recombination in Quantum Dot Sensitized Solar Cells. *Acc. Chem. Res.* **2009**, *42*, 1848−1857.

(2) Yu, W. W.; Qu, L.; Guo, W.; Peng, X. Experimental Determination of the Extinction Coefficient of CdTe, CdSe, and CdS Nanocrystals. *Chem. Mater.* **2003**, *15*, 2854−2860.

(3) Wang, P.; Zakeeruddin, S. M.; Moser, J. E.; Humphry-Baker, R.; Comte, P.; Aranyos, V.; Hagfeldt, A.; Nazeeruddin, M. K.; Grätzel, M. Stable New Sensitizer with Improved Light Harvesting for Nanocrystalline Dye-Sensitized Solar Cells. *Adv. Mater.* **2004**, *16*, 1806−1811.

(4) Vogel, R.; Pohl, K.; Weller, H. Sensitization of Highly Porous, Polycrystalline TiO_2 Electrodes by Quantum Sized CdS. *Chem. Phys. Lett.* **1990**, *174*, 241−246.

(5) Vogel, R.; Hoyer, P.; Weller, H. Quantum-Sized PbS, CdS, Ag_2S, Sb_2S_3, and Bi_2S_3 Particles as Sensitizers for Various Nanoporous Wide-Bandgap Semiconductors. *J. Phys. Chem.* **1994**, *98*, 3183−3188.

(6) Schaller, R. D.; Sykora, M.; Pietryga, J. M.; Klimov, V. I. Seven Excitons at a Cost of One: Redefining the Limits for Conversion Efficiency of Photons into Charge Carriers. *Nano Lett.* **2006**, *6*, 424−429.

(7) Trinh, M. T.; Houtepen, A. J.; Schins, J. M.; Hanrath, T.; Piris, J.; Knulst, W.; Goossens, A. P.; Siebbeles, L. D. In spite of Recent Doubts Carrier Multiplication Does Occur in PbSe Nanocrystals. *Nano Lett.* **2008**, *8*, 1713−1718.

(8) Beard, M. C.; Luther, J. M.; Semonin, O. E.; Nozik, A. J. Third Generation Photovoltaics Based on Multiple Exciton Generation in Quantum Confined Semiconductors. *Acc. Chem. Res.* **2013**, *46*, 1252−1260.

(9) Nozik, A. J. Nanoscience and Nanostructures for Photovoltaics and Solar Fuels. *Nano Lett.* **2010**, *10*, 2735−2741.

(10) Stewart, J. T.; Padilha, L. A.; Qazilbash, M. M.; Pietryga, J. M.; Midgett, A. G.; Luther, J. M.; Beard, M. C.; Nozik, A. J.; Klimov, V. I. Comparison of carrier Multiplication Yields in PbS and PbSe Nanocrystals: the Role of Competing Energy-Loss Processes. *Nano Lett.* **2012**, *12*, 622−628.

(11) Hanna, M. C.; Beard, M. C.; Nozik, A. J. Effect of Solar Concentration on the thermodynamic Power Conversion Efficiency of Quantum-Dot Solar Cells Exhibiting Multiple Exciton Generation. *J. Phys. Chem. Lett.* **2012**, *3*, 2857−2862.

(12) Nozik, A. Quantum Dot Solar Cells. *Phys. E* **2002**, *14*, 115−120.

(13) Nozik, A. Exciton Multiplication and Relaxation Dynamics in Quantum Dots: Applications to Ultrahigh-Efficiency Solar Photon Conversion. *Inorg. Chem.* **2005**, *44*, 6893−6899.

(14) Kongkanand, A.; Tvrdy, K.; Takechi, K.; Kuno, M.; Kamat, P. V. Quantum Dot Solar Cells. Tuning Photoresponse Through Size and Shape Control of CdSe-TiO_2 Architecture. *J. Am. Chem. Soc.* **2008**, *130*, 4007−4015.

(15) Leschkies, K. S.; Divakar, R.; Basu, J.; Enache-Pommer, E.; Boercker, J. E.; Carter, C. B.; Kortshagen, U. R.; Norris, D. J.; Aydil, E. S. Photosensitization of ZnO Nanowires with CdSe quantum Dots for Photovoltaic Devices. *Nano Lett.* **2007**, *7*, 1793−1798.

(16) Duan, J.; Zhang, H.; Tang, Q.; He, B.; Yu, L. Recent Advances in Critical Materials for Quantum Dot-Sensitized Solar Cells: A Review. *J. Mater. Chem. A* **2015**, *3*, 17497−17510.

(17) Pan, Z.; Mora-Sero, I.; Shen, Q.; Zhang, H.; Li, Y.; Zhao, K.; Wang, J.; Zhong, X.; Bisquert, J. High-Efficiency "Green" Quantum Dot Solar Cells. *J. Am. Chem. Soc.* **2014**, *136*, 9203−10.

(18) Chen, C.; Ali, G.; Yoo, S. H.; Kum, J. M.; Cho, S. O. Improved Conversion Efficiency of CdS Quantum Dot-Sensitized TiO_2 Nanotube-Arrays Using $CuInS_2$ as a Co-Sensitizer and an Energy Barrier Layer. *J. Mater. Chem.* **2011**, *21*, 16430−16435.

(19) Wang, J.; Mora-Seró, I.; Pan, Z.; Zhao, K.; Zhang, H.; Feng, Y.; Yang, G.; Zhong, X.; Bisquert, J. Core/shell Colloidal Quantum Dot Exciplex States for the Development of Highly Efficient Quantum-Dot-Sensitized Solar Cells. *J. Am. Chem. Soc.* **2013**, *135*, 15913−15922.

(20) Pan, Z.; Zhao, K.; Wang, J.; Zhang, H.; Feng, Y.; Zhong, X. Near Infrared Absorption of $CdSe_x$ Te_{1-x} Alloyed Quantum Dot Sensitized Solar Cells with More than 6% Efficiency and High Stability. *ACS Nano* **2013**, *7*, 5215−5222.

(21) Mathew, S.; Yella, A.; Gao, P.; Humphry-Baker, R.; Curchod, B. F.; Ashari-Astani, N.; Tavernelli, I.; Rothlisberger, U.; Nazeeruddin, M. K.; Grätzel, M. Dye-Sensitized Solar Cells with 13% Efficiency Achieved Through the Molecular Engineering of Porphyrin Sensitizers. *Nat. Chem.* **2014**, *6*, 242−247.

(22) Chakrapani, V.; Baker, D.; Kamat, P. V. Understanding the Role of the Sulfide Redox Couple (S^{2-}/S_n^{2-}) in Quantum Dot-Sensitized Solar Cells. *J. Am. Chem. Soc.* **2011**, *133*, 9607−9615.

(23) Kamat, P. V. Boosting the Efficiency of Quantum Dot Sensitized Solar Cells Through Modulation of Interfacial Charge Transfer. *Acc. Chem. Res.* **2012**, *45*, 1906−1915.

(24) Ellis, A. B.; Kaiser, S. W.; Bolts, J. M.; Wrighton, M. S. Study of n-Type Semiconducting Cadmium Chalcogenide-Based Photoelectrochemical Cells Employing Polychalcogenide Electrolytes. *J. Am. Chem. Soc.* **1977**, *99*, 2839−2848.

(25) Bang, J. H.; Kamat, P. V. Quantum Dot Sensitized Solar Cells. A Tale of Two Semiconductor Nanocrystals: CdSe and CdTe. *ACS Nano* **2009**, *3*, 1467−1476.

(26) Haydous, F.; Halaoui, L. Quantum-Confined CdTe Films Deposited by SILAR and Their Photoelectrochemical Stability in the Presence of Se^{2-} as a Hole Scavenger. *J. Phys. Chem. C* **2014**, *118*, 18334−18342.

(27) Samadpour, M.; Irajizad, A.; Taghavinia, N.; Molaei, M. A New Structure to Increase the Photostability of CdTe Quantum Dot Sensitized Solar Cells. *J. Phys. D: Appl. Phys.* **2011**, *44*, 045103.

(28) Nishimura, S.; Shishido, A.; Abrams, N.; Mallouk, T. E. Fabrication Technique for Filling-Factor Tunable Titanium Dioxide Colloidal Crystal Replicas. *Appl. Phys. Lett.* **2002**, *81*, 4532−4534.

(29) Nishimura, S.; Abrams, N.; Lewis, B. A.; Halaoui, L. I.; Mallouk, T. E.; Benkstein, K. D.; van de Lagemaat, J.; Frank, A. J. Standing Wave Enhancement of Red Absorbance and Photocurrent in Dye-Sensitized Titanium Dioxide Photoelectrodes Coupled to Photonic Crystals. *J. Am. Chem. Soc.* **2003**, *125*, 6306−6310.

(30) Kamat, P. V.; Patrick, B. Photophysics and Photochemistry of Quantized Zinc Oxide Colloids. *J. Phys. Chem.* **1992**, *96*, 6829−6834.

(31) Chestnoy, N.; Harris, T.; Hull, R.; Brus, L. Luminescence and Photophysics of Cadmium Sulfide Semiconductor Clusters: the Nature of the Emitting Electronic State. *J. Phys. Chem.* **1986**, *90*, 3393−3399.

(32) de Mello Donega, C.; Koole, R. Size Dependence of the Spontaneous Emission Rate and Absorption Cross Section of CdSe and CdTe Quantum Dots. *J. Phys. Chem. C* **2009**, *113*, 6511−6520.

(33) Kamal, J. S.; Omari, A.; Van Hoecke, K.; Zhao, Q.; Vantomme, A.; Vanhaecke, F.; Capek, R. K.; Hens, Z. Size-Dependent Optical

DOI: 10.1021/acs.jpcc.5b11478
J. Phys. Chem. C 2016, 120, 4766−4778

Properties of Zinc Blende Cadmium Telluride Quantum Dots. *J. Phys. Chem. C* **2012**, *116*, 5049−5054.
(34) Landes, C.; Burda, C.; Braun, M.; El-Sayed, M. Photoluminescence of CdSe Nanoparticles in the Presence of a Hole Acceptor: n-Butylamine. *J. Phys. Chem. B* **2001**, *105*, 2981−2986.
(35) Sharma, S. N.; Pillai, Z. S.; Kamat, P. V. Photoinduced Charge Transfer Between CdSe Quantum Dots and p-Phenylenediamine. *J. Phys. Chem. B* **2003**, *107*, 10088−10093.
(36) Wei, S.-H.; Zunger, A. Calculated Natural Band Offsets of all II−VI and III−V Semiconductors: Chemical Trends and the Role of Cation d Orbitals. *Appl. Phys. Lett.* **1998**, *72*, 2011.
(37) Yu, K.; Zaman, B.; Romanova, S.; Wang, D. s.; Ripmeester, J. A. Sequential Synthesis of Type II Colloidal CdTe/CdSe Core−Shell Nanocrystals. *Small* **2005**, *1*, 332−338.
(38) Kim, S.; Fisher, B.; Eisler, H.-J.; Bawendi, M. Type-II Quantum Dots: CdTe/CdSe (Core/Shell) and CdSe/ZnTe (Core/Shell) Heterostructures. *J. Am. Chem. Soc.* **2003**, *125*, 11466−11467.
(39) Samanta, A.; Deng, Z.; Liu, Y. Aqueous Synthesis of Glutathione-Capped CdTe/CdS/ZnS and CdTe/CdSe/ZnS Core/Shell/Shell Nanocrystal Heterostructures. *Langmuir* **2012**, *28*, 8205−8215.
(40) Chuang, C.; Lo, S. S.; Scholes, G. D.; Burda, C. Charge Separation and Recombination in CdTe/CdSe Core/Shell Nanocrystals as a Function of Shell Coverage: Probing the Onset of the Quasi Type-II Regime. *J. Phys. Chem. Lett.* **2010**, *1*, 2530−2535.
(41) Lo, S. S.; Mirkovic, T.; Chuang, C.; Burda, C.; Scholes, G. D. Emergent Properties Resulting from Type-II Band Alignment in Semiconductor Nanoheterostructures. *Adv. Mater.* **2011**, *23*, 180−197.
(42) Henglein, A. Photo-Degradation and Fluorescence of Colloidal-Cadmium Sulfide in Aqueous Solution. *Ber. Bunsen-Ges. Phys. Chem.* **1982**, *86*, 301−305.
(43) Resch, U.; Weller, H.; Henglein, A. Photochemistry and radiation chemistry of colloidal semiconductors. 33. Chemical Changes and Fluorescence in CdTe and ZnTe. *Langmuir* **1989**, *5*, 1015−1020.
(44) El Harakeh, M.; Halaoui, L. Enhanced Conversion of Light at TiO_2 Photonic Crystals to the Blue of a Stop Band and at TiO_2 Random Films Sensitized with Q-CdS: Order and Disorder. *J. Phys. Chem. C* **2010**, *114*, 2806−2813.
(45) Bayram, S.; Halaoui, L. Amplification of Solar Energy Conversion in Quantum-Confined CdSe-Sensitized TiO_2 Photonic Crystals by Trapping Light. *Part. Part. Syst. Char.* **2013**, *30*, 706−714.
(46) Gao, X.-F.; Li, H.-B.; Sun, W.-T.; Chen, Q.; Tang, F.-Q.; Peng, L.-M. CdTe Quantum Dots-Sensitized TiO_2 Nanotube Array Photoelectrodes. *J. Phys. Chem. C* **2009**, *113*, 7531−7535.

DOI: 10.1021/acs.jpcc.5b11478
J. Phys. Chem. C 2016, 120, 4766−4778